Analysis of microstructure, deformation and permeability of salt/sand mixtures during creep

Shen, X.[1], Zhu, C.[2], Arson, C.[1]

[1]School of Civil and Environmental Engineering, Georgia Institute of Technology, Atlanta, Georgia, 790 Atlantic Drive; email: chloe.arson@ce.gatech.edu
[2] Bureau of Economic Geology, University of Texas at Austin

ABSTRACT

The impact of impurities on salt healing properties is studied through creep tests performed on brine saturated granular salt with various quartz contents. Quartz grains act as shields that reduce dissolution at salt grain contacts and decrease the creep rate. Non-smooth creep curves are obtained for specimens with 50% quartz contents, due to sequential pore collapse. Micro-CT images acquired before creep, after creep, and after unloading, show that pore-to-pore distances decrease with quartz contents and that the creep rate decreases as the mean area of the salt grain contacts increases. Based on grain scale thermodynamic models, we show that creep deformation is controlled by diffusion - not dissolution-precipitation. Permeability evolution is less sensitive to porosity than to void radius and spacing, which control pore connectivity. The proposed modeling framework can be used in any crystalline material to relate microscopic reaction rates to macroscopic deformation rates.

INTRODUCTION

Salt rock is of great potential for geological storage because of its low permeability and favorable creep properties. During creep, stresses at grain contacts can trigger dissolution, salt ion transport through fluid films, and re-precipitation at low-stress grain boundaries. This phenomenon, known as pressure-solution, can occur in the same conditions of pressure and temperature as grain boundary diffusion. Micro-computed tomography (micro-CT) was used to interpret fabric development and explain macroscopic mechanical damage and healing in salt (Gaye et al., 2014). Geometrical models were proposed to capture the increase of salt permeability that occurs at almost constant porosity during crack propagation (Peach and Spiers, 1996). In halite, the controlling pressure solution mechanism is determined by solubility and dissolution rates, mineral sizes, and the geometry of grain contacts (Pluymakers and Spiers 2014). Few researchers studied the impact of impurities on salt healing potential (Hickman and Evans, 1991). The present work focuses on granular mixtures with variable contents of salt (NaCl) and quartz (SiO_2). After describing the creep tests, we analyze microstructure CT scan images and present micro-macro models of creep deformation and permeability evolution.

CREEP TESTS ON SALT-SAND MIXTURES

Creep tests were conducted at ambient temperature on mixtures of salt grains (ranging between 180 μm and 212 μm in size) and quartz grains (about 500 μm in size) saturated with brine. The initial porosity of the specimens (before the creep load was applied) was 40%. Materials with three different solid volume fractions were tested: 100% salt; 75% salt – 25% quartz, 50% salt – 50% quartz. The setup is presented in Fig.1(a). Specimens were contained in acrylic tubes with an inner diameter of 0.63 cm and a length of 2.5 cm, which ensured that each sample had a representative number of grains (about 50,000). Salt and quartz grains were weighted, mixed and poured into the acrylic tubes through a funnel. Acrylic rods were placed at both ends of the samples to transfer external stress. A 1.675 kg steel rod was placed on the top acrylic rod, which allowed applying a stress of 1.65 MPa to the sample. The acrylic tubes were then immersed in small tanks full of brine. The tubes were at constant fluid pressure (drained) at the top and bottom. Due to capillary forces, samples were saturated in 5 seconds. The vertical strain of the sample was measured by using a Linear Variable Differential Transformer (LVDT) throughout the tests, which lasted 3.5 hr. The steel rod and the LVDTs were held by a clamp and the whole set up was placed in an environmental chamber to maintain temperature and humidity constant. Fig.1(b) shows the evolution of the axial strain for the different mixtures. Each creep tests was performed twice or three times (experiments 1,2, 3 in Fig.1.b). Differences in final axial strain were less than 8%, which shows that the tests were repeatable.

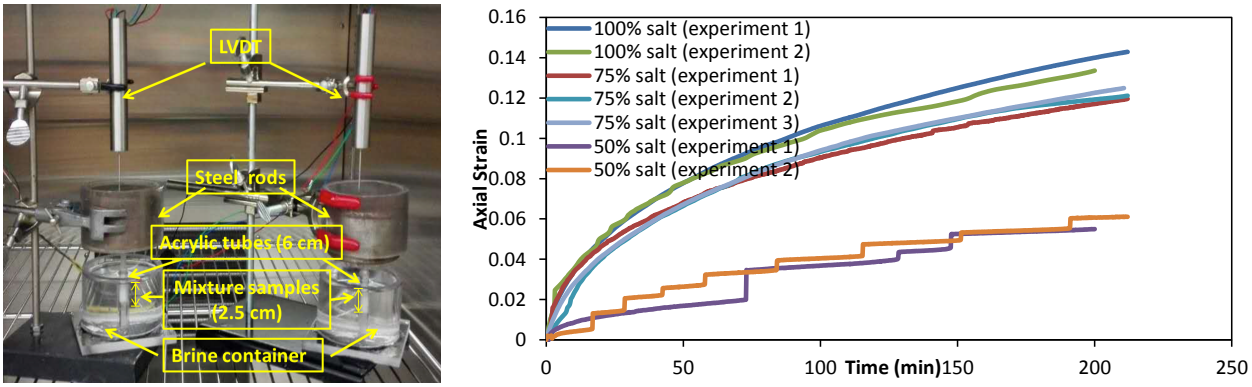

a. Creep test set-up. b. Time evolution of axial strain during creep tests.

Figure 1. Creep tests conducted on salt/quartz mixtures at 100%, 75% and 50% salt.

Axial strain accumulates with time according to a logarithmic function. The strain rate and final cumulated deformation were higher at higher salt contents. By contrast, Hickerman and Evans (1991) noted that grain-to-grain distances did not shorten at measurable rate at salt-to-salt contacts, and observed grain-to-grain distance shortening at salt-to-quartz contacts only. Creep curves for the specimens at 50% quartz were not smooth, which may be due to the collapse of large voids during the creep consolidation process. However, according to the microstructure image analyses presented in the following (Fig.3), samples with 50% quartz contents had a more uniform void size distribution, centered around smaller void sizes, than the other specimens.

MICROSTRUCTURE CT SCAN IMAGE ACQUISITION AND ANALYSIS

We used a micro-CT Scanning system to reconstruct 3D images of samples' microstructure at three key stages of the creep test: in dry conditions, before the creep load is applied; in brine saturated conditions, at the end of the creep test; in brine saturated conditions, after the creep load has been removed. For brine-saturated samples, epoxy resin was used to seal the acrylic rods to the acrylic tubes and maintain samples' water contents and length. We conducted statistical analyses of 2D microstructure descriptors of longitudinal and cross-sectional images of the samples. Table 1 shows the 8 CT scans obtained in this study.

Table. 1 CT scanning images.

(*) Pixel size: 20 μm*20 μm, distance between slices: 20 μm, length of scanned sample: 1 cm.

(#) Pixel size: 15 μm*15 μm, distance between slices: 15 μm, length of scanned sample: 0.6 cm.

Solid contents	Before creep test (dry conditions)	After saturated creep test	After saturated creep test and unloading
100% salt 0% quartz	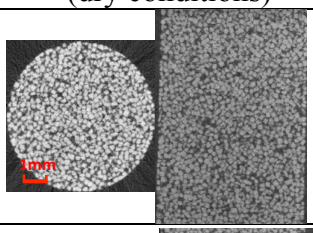 *	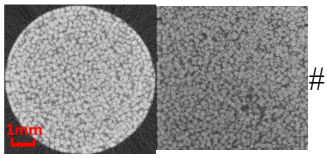 #	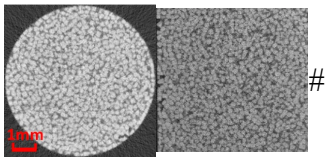 #
75% salt 25% quartz	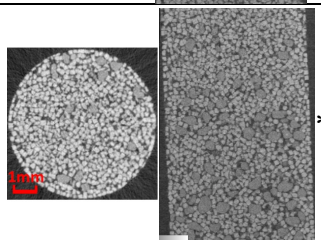 *	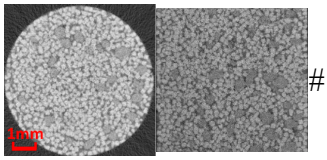 #	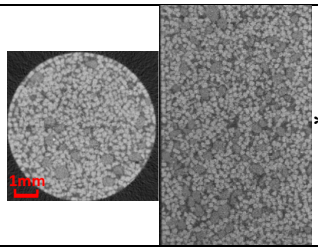 *
50% salt 50% quartz	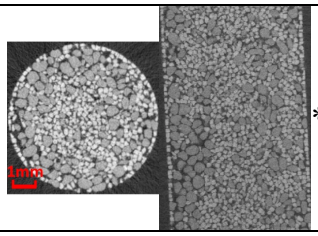 *	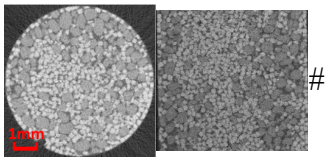 #	

Probability density functions (pdfs) of void to void distances were similar in cross sectional and longitudinal images. Distances between voids were smaller at higher quartz contents. The higher probability of void connectivity induces a lower probability of grain contact, which may explain the lower creep rate measured at high quartz content. Before the creep tests, the pdf of void-to-void distances was normal in samples with 0% and 25% quartz, and log-normal in samples with 50% quartz (Fig.2). After the saturated creep test and before unloading, centroid-to-centroid distances decreased in all mixtures due to pressure solution. The pdf was normal in samples with 0% quartz, and log-normal in samples with 25% and 50% quartz. Similar results were obtained before and after unloading, indicating that elastic microstructure changes were minimal. This observation is in agreement with published experimental studies (Spiers et al., 1990), which show that initial compaction has no measurable influence on the creep response of wet granular

salt. More tests will be done to check whether or not instantaneous strains influence creep deformation. Void areas followed a power law distribution in all mixtures, both before and after creep (Fig.3). During the creep tests, the larger voids disappeared and the number of smaller voids increased, particularly in mixtures with higher quartz contents. We will improve the mixing technique to avoid large particle clustering and check these results.

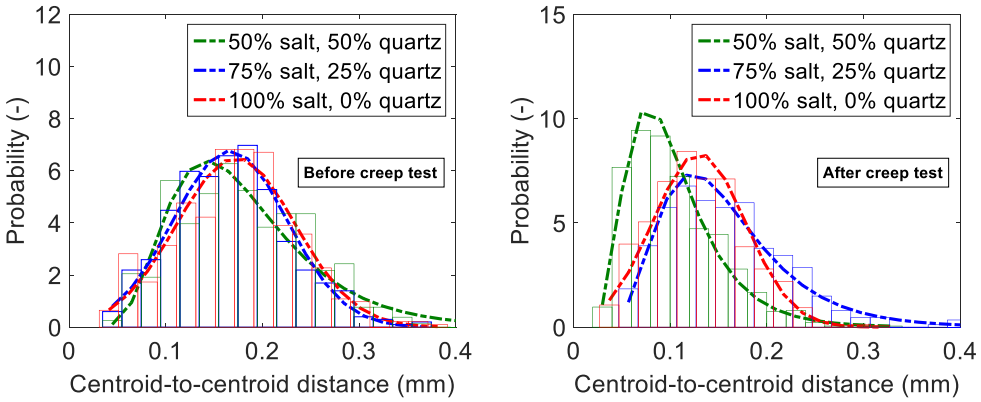

Figure 2. Pdfs of 2D void-to-void distances before (left) and after (right) the creep tests.

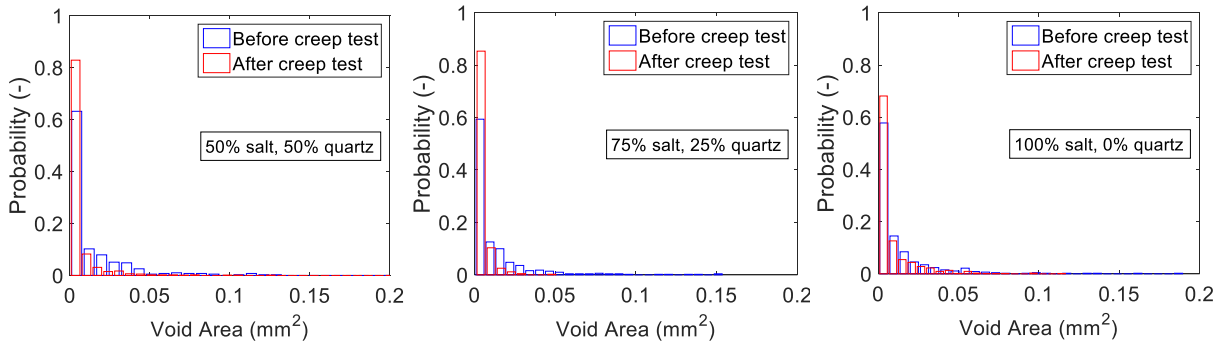

Figure 3. Pdfs of void areas before creep and after the creep (before unloading).

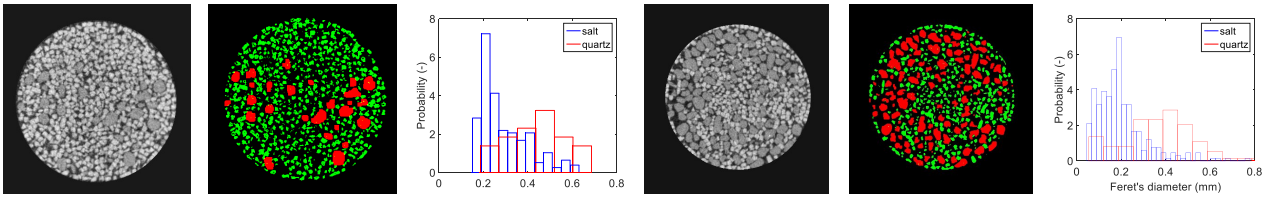

Figure 4. Bimodal size distribution of solid grains before the creep loading test (left: 75% salt, 25% quartz; right: 50% salt, 50% quartz).

The density contrast between solid particles was enhanced to obtain the salt and quartz grain size distributions (GSDs). Grain sizes were measured by Feret's diameter. Mixtures' GSDs are clearly bimodal (Fig.4): Salt GSD is lognormal, with a typical particle size of 0.2 mm, and quartz GSD is normal, with a typical particle size of 0.5 mm. Due to pressure solution, salt boundaries changed shape and boundary gaps closed. Although the grain boundary detection technique still needs improvement, visual observation of both lateral and longitudinal images revealed that during creep, the number of salt grain clusters increased and pore size decreased dramatically.

CHEMICAL EVOLUTION OF MICROSTRUCTURE AND INFLUENCE ON CREEP RATE AND PERMEABILITY

Microstructure-based model of pressure solution creep

Considering that flat grain-to-grain contacts are separated by a thin fluid film, an increase of effective stress in the solid skeleton causes a drop in the normal component of the solid chemical potential at grain contacts (Pluymakers and Spiers 2014), as follows:

$$\Delta\tilde{\mu}_n \approx \left(\tilde{\sigma}_n - P_f\right)\Omega \approx \frac{\sigma_n^e \Omega d_s}{a_c} \tag{1}$$

Where $\tilde{\sigma}_n$ is the local mean normal stress acting on a given grain boundary, P_f is the pore fluid pressure acting on the free pore walls, σ_n^e is the applied effective stress, d_s is the grain center – to – grain center distance, a_c is the contact area and Ω is the molar volume. Due to the difference of chemical potential, the material dissolves at compressed grain contacts, diffuses along the grain boundaries and precipitates on free pore walls. Dissolution-precipitation and diffusion velocities (V_{dp} and V_{dif}) are expressed as:

$$V_{dp} = I_{dp}\frac{\sigma_n^e \Omega d_s^2}{RTa_c} \qquad V_{dif} = \frac{2\pi DC_0 S\Omega}{\beta a_c}\frac{\sigma_n^e \Omega d_s^2}{RTa_c} \tag{2}$$

In which I_{dp} is a velocity coefficient. Table 2 summarizes the model parameters: D is the grain boundary diffusion coefficient; C_0 is the mean concentration of dissolved solid at grain boundaries; S is the mean fluid film thickness; β is a geometric factor of the order 0.5. If the contact area is larger (respectively smaller) than a critical area threshold a_c^* (Shen et al., 2016):

$$a_c^* = \frac{2\pi DC_0 S\Omega}{\beta I_p} \tag{3}$$

then V_{dp} is larger (respectively smaller) than V_{dif} and the local pressure solution phenomenon is diffusion controlled (respectively dissolution-precipitation controlled).

Table 2. Pressure solution parameters.

	C_0 (mol/L)	$D(m^2/s)$	S(nm)	$\Omega(m^3/mol)$	$I_{dp}(m/s)$
NaCl	6.48	1.3×10^{-9}	20	2.7×10^{-5}	1×10^{-2}
SiO_2	1×10^{-4}	7×10^{-10}	20	2.3×10^{-5}	1×10^{-15}

We assume that grains are initially spherical and that upon pressure solution, spherical caps at the grain contacts are dissolved to form flat grain-to-grain contacts. When the contact area (a_c) increases, more salt is dissolved, which decreases the grain center to grain center distance (d_s), the volume of solid salt (V_s) and the sample volume (V_t). The corresponding volume changes are:

$$\delta V_s = \left(\frac{4Z\left(d_p - \sqrt{d_p^2 - 4a_c/\pi}\right)\left(2d_p + \sqrt{d_p^2 - 4a_c/\pi}\right)}{6\sqrt{d_p^2 - 4a_c/\pi}} - \frac{2Z\left(d_p - \sqrt{d_p^2 - 4a_c/\pi}\right)^2}{6\sqrt{d_p^2 - 4a_c/\pi}}\right)\delta a_c, \quad \delta V_t = d_p \delta d_s \tag{4}$$

Where Z is the coordination number. According to the model presented in (Pluymakers and Spiers 2014), and using the parameters listed in Table 2, the axial strain that would be obtained in a saturated quartz sample subjected to a 1.65MPa vertical stress for 3.5hrs at ambient

temperature is 1.8×10^{-9}, which is negligible compared the strains obtained in the salt mixtures. Hence, we neglect the pressure solution phenomena that occur in the quartz grains. The reduced number of contact points under compressive stress in the salt grains correlates with slower pressure solution in mixtures with higher quartz contents (Fig.2). In order to capture the attenuation of creep at higher quartz contents, we express the axial strain rate of the salt/sand mixtures as a fraction of the strain rate of granular salt. The scaling factor is noted η. We calibrate the mean of the initial distribution of salt grain contact areas and the scaling parameter against the experimental creep curves. The calibration results (Table 3) are consistent with the assumption formulated above: The presence of quartz in the samples reduces the number of contact forces applied to salt grains, but the area of the contact surfaces on salt grains increases with quartz contents, which, according to the model, results in smaller strain rates.

Table 3. Calibrated parameters of the pressure-solution creep model.

	100% salt	75% salt	50% salt
Mean of the initial distribution of salt grain contact areas (m^2)	2.826×10^{-9}	3.22×10^{-9}	4.07×10^{-9}
η	1	0.9	0.5

Impact of the chemical evolution of microstructure on permeability

We model the voids in the granular assembly as 3D spheroids. For an isotropic distribution of spheroidal voids that are characterized by independent and narrow pdfs of radius (R), aperture (λ) and spacing (L), the intrinsic permeability is (Guéguen and Dienes 1989):

$$k = \frac{4\pi}{15} f \frac{\bar{\lambda}^3 \bar{R}^2}{\bar{l}^3} \tag{5}$$

In which $\bar{\lambda}$ is the average half-spheroid aperture, $\bar{R}$ is the average spheroid radius, $\bar{l}$ is the average void spacing. The connectivity factor f characterizes the fraction of voids that passed the percolation threshold. Percolation occurs after a critical crack void number density is reached. The projection of an orderly-packed granular salt assembly in 2D suggests that each void has a maximum number of four neighboring voids. Thus we calculated the parameter f by representing the porous network as a four-fold Bethe lattice and by using the concept of excluded volume between two discs. Permeability can be expressed as follows:

$$k = \frac{4\pi}{15} \frac{\bar{\lambda}^3 \bar{R}^2}{\bar{l}^3} \left\{ 1 - 4 \left[\sqrt{\frac{4\bar{l}^3}{\pi^2 \bar{R}^3}} - \frac{3}{4} - \frac{1}{2} \right]^3 + 3 \left[\sqrt{\frac{4\bar{l}^3}{\pi^2 \bar{R}^3}} - \frac{3}{4} - \frac{1}{2} \right]^4 \right\} \tag{6}$$

SENSITIVITY ANALYSIS

Microstructure-based model of pressure solution creep

The impact of the initial mean contact area on creep strain with η equals to 1 and a fixed standard deviation of $8.23 \times 10^{-19} m^2$ is illustrated in Figure 5.a. Axial strain accumulated during creep is larger when the initial mean contact area is smaller (mac, in m^2). The time evolution of

the distribution of contact areas during saturated creep tests is showed in Figure 5.b, for a lognormal distribution of initial contact areas with a fixed mean value of $2.83 \times 10^{-9} m^2$ and a fixed standard deviation of $8.23 \times 10^{-19} m^2$. Grain contact areas increase due to pressure solution. With the given parameters (Table 2), the threshold contact area a_c^* for salt is 6.3114×10^{-15} m^2. The probability that the contact area be smaller than a_c^* is negligible (Fig.5.b), which implies that creep tests were controlled by diffusion. Ultimately, all contact areas are larger than a_c^*, the strain rate is diffusion controlled and contact areas follow a uniform distribution.

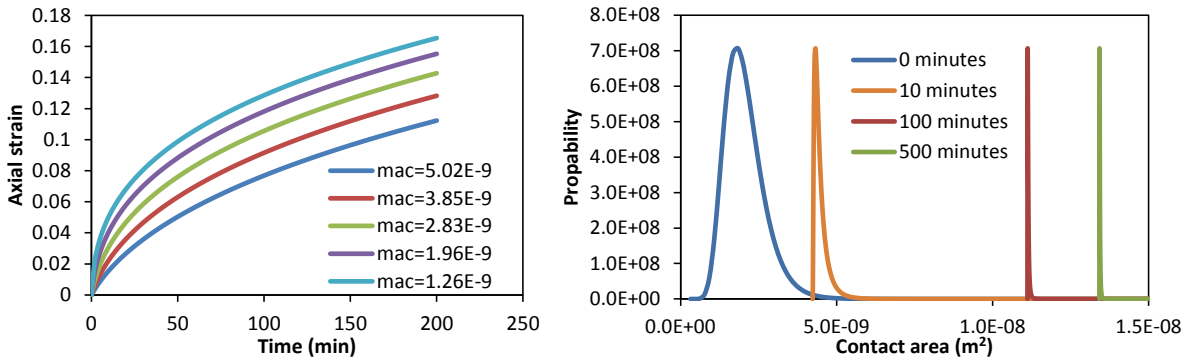

(a) Impact of initial mean contact area on creep strain (b) Evolution of contact area distribution

Figure 5. Sensitivity of the creep model to the distribution of salt grain contact areas.

Impact of the chemical evolution of microstructure on permeability

Sensitivity analyses confirm that for a fixed number of pores, a larger void aperture, a larger void radius or a smaller void spacing increases permeability (Fig.6). For similar relative changes, permeability is most sensitive to void spacing and least sensitive to void aperture. The volume of the porous space has no influence on permeability below the percolation threshold. Permeability changes are controlled by changes in void connectivity, which dominate changes of porosity. According to the image analysis presented above, when quartz contents increases, the area of voids increases and the pore-to-pore distances decrease, which results in higher permeability.

CONCLUSIONS

Results of creep tests performed at ambient temperature on brine saturated salt-quartz granular mixtures show that quartz grains act as shields that reduce dissolution at salt grain contacts and decrease the creep rate. Non-smooth creep curves were obtained for specimens with 50% quartz contents, which was attributed to sequential pore collapse. The statistical analysis of cross sectional and longitudinal images of CT scan images indicated that pore-to-pore distances decrease with quartz contents. A micro-macro model of creep deformation and permeability evolution is proposed. We show that the creep tests presented here are controlled by diffusion, not precipitation-dissolution. The axial strain rate increases when the initial contact area decreases, and over time, contact areas increase due to pressure solution. Compared to porosity, pore connectivity, governed mostly by void radius and spacing, dominated the evolution of permeability. The proposed framework can be used in any crystalline material to relate microscopic reaction rates to macroscopic deformation rates.

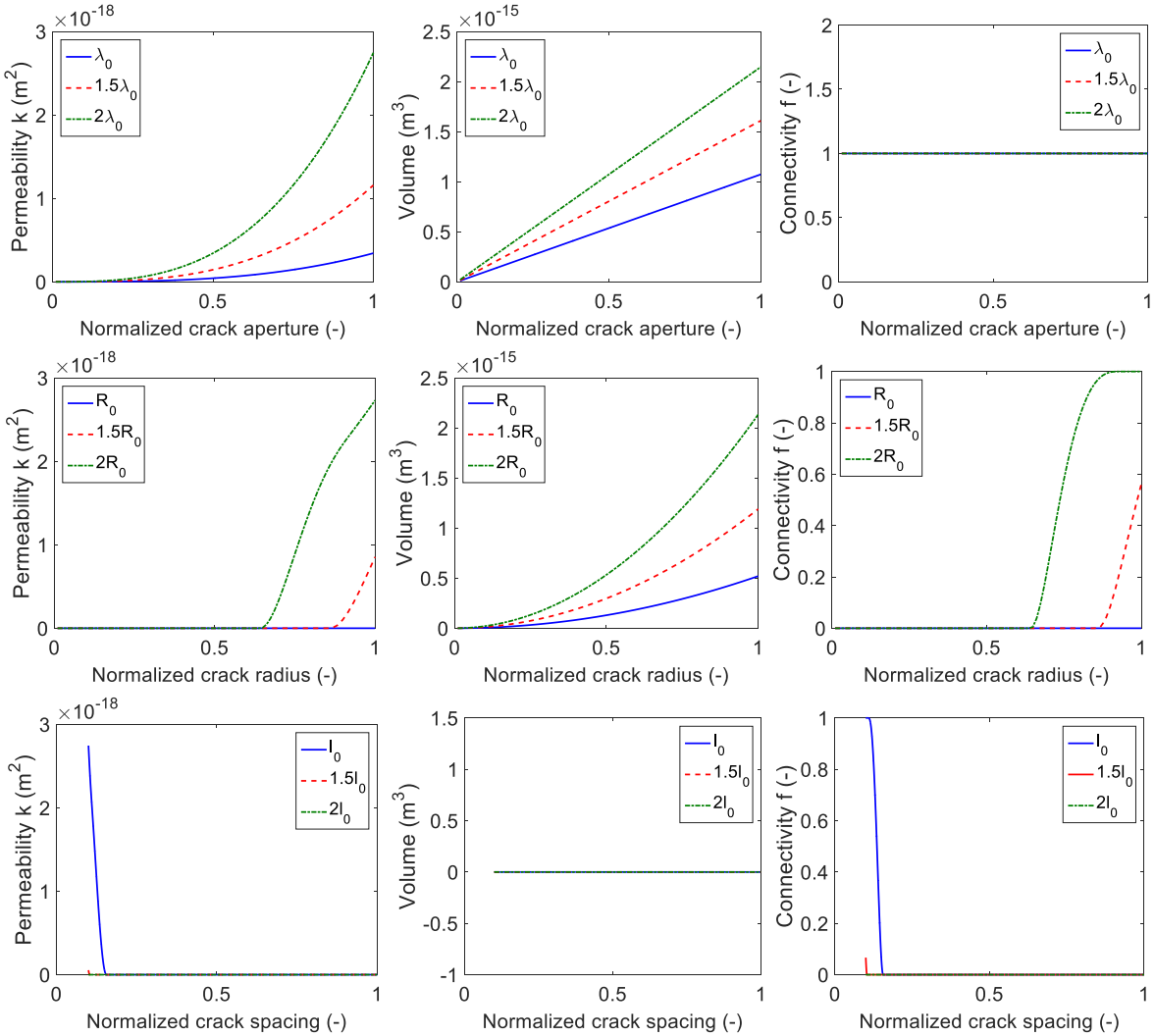

Figure 6. Influence of spheroidal void aperture, radius and spacing on permeability.

ACKNOWLEDGEMENTS: Research supported by the National Science Foundation (CMMI-1362004/1361996).

REFERENCES

Gaye, A., Bornert, M., Lenoir, N., Sab, K., Dimanov, A., Bourcier, M., ... & Ludwig, W. (2014). Micromechanics of Halite Investigated by 2D and 3D Multiscale Full-Field Measurements. In 48th ARMA Symposium.

Guéguen, Y. and J. Dienes. (1989). Transport properties of rocks from statistics and percolation. *Mathematical Geology*. 21 (1): 1-13.

Hickman, S.H. and Evans, B. (1991). *Experimental pressure solution in halite: the effect of grain/interphase boundary structur*e, Journal of the Geological Society, V148, 459-460.

Peach, C. J., & Spiers, C. J. (1996). Influence of crystal plastic deformation on dilatancy and permeability development in synthetic salt rock. *Tectonophysics*, *256*(1), 101-128.

Pluymakers, A. and Spiers, C. J. (2014). *Compaction creep of simulated anhydrite fault gouge by pressure solution: theory vs. experiments and implications for fault sealing*, Geological Society, London, 409, SP409-6.

Shen, X., Zhu, C., Arson, C. (2016). *Chemo-mechanical damage and healing of granular salt: micro-macro modeling*, In 50th ARMA Symposium.

Shimizu I. (1995). *Kinetics of pressure solution creep in quartz: theoretical considerations*, Tectonophysics 245 121-134.

Spiers, C. J., Schutjens, P. M. T. M., Brzesowsky, R. H., Peach, C. J., Liezenberg, J. L., & Zwart, H. J. (1990). Experimental determination of constitutive parameters governing creep of rocksalt by pressure solution. *Geological Society, London, Special Publications*, *54*(1), 215-227.